Analyst

COMMUNICATION

Dual conical shell illumination for volumetric high-energy X-ray diffraction imaging

Anthony Dicken,[a] Daniel Spence,[a] Keith Rogers,[b] Danae Prokopiou,[b] and Paul Evans [a*]

Received 00th January 20xx,
Accepted 00th January 20xx

DOI:
10.1039/x0xx00000xwww.rsc.org/

To retrieve crystallographic information from extended sample volumes requires a high-energy probe. The use of X-rays to combine imaging with materials characterisation is well-established. However, if fundamental crystallographic parameters are required, then the collection and analysis of X-rays diffracted by the inspected samples are prerequisites. We present a new X-ray diffraction imaging architecture, which in comparison with previous depth-resolving hollow beam techniques requires significantly less X-ray power or alternatively supports significantly increased scanning speeds. Our conceptual configuration employs a pair of conical shell X-ray beams derived from a single point source to illuminate extended samples. Diffracted flux measurements would then be obtained using a pair of energy resolving point detectors. This dual beam configuration is tested using a single X-ray beam set-up employing a dual scan. The use of commercial off-the-shelf low-cost components has the potential to provide rapid and cost-effective performance in areas including industrial process control, medical imaging and explosives detection.

The highly penetrative nature of X-rays led directly to their chance discovery,[1]. This property coupled with their interaction on an atomic and molecular scale to produce crystallographic, structurally dependent scattering has fuelled new scientific discoveries and instrumentation for well over a century. For example, X-ray based probes have proliferated into a wealth of important non-destructive imaging modalities capitalising upon different X-ray interaction mechanisms including; X-ray spectroscopy,[2] X-ray diffraction (XRD),[3-7] coherent scattering,[8] and phase contrast,[9]. Many applications would benefit from the information provided by these probes attributed to material phases distributed within an inspection volume. In response, these techniques have also been developed into tomographic modalities on the >mm length scale. X-ray diffraction tomography has become the preeminent technique for structural imaging as it provides simultaneously crystallographic data from materials phases distributed within volumes,[10]. Various implementation strategies have been investigated including; 3DXRD,[11] TEDDI,[12-13] XDI,[14] and SICSI,[10] and have all been individually adapted to their application. Angular-dispersive X-ray diffraction is exploited in the 3DXRD method to provide high-fidelity structural measurement that includes capabilities such as mapping the position, volume, orientation and stress state in grain boundaries. This additional functionality comes at the expense of acquisition speed (potentially several hours for a data collection) necessitating in practice a synchrotron source. Most techniques adopt an energy-dispersive approach (though SICSI may be considered as an angle/energy dispersive hybrid) to provide an increase in the diffracted flux thereby reducing data collection times. Typically, the beam geometries employed involve collimating photons to produce narrow slit or pencil beams either pre or post sample thus restricting the scattered flux available for measurement. This limitation coupled with low scattering cross-sections or probabilities of interaction is especially problematic when using high X-ray energies to penetrate extended samples. In practice, these scientific and operational challenges are addressed with limited success using significantly brighter X-ray sources or longer scan times. Specifically, our work is driven by the time critical operational challenges encountered in many industrial screening processes. The requirement for information such as the spatial distribution of specific material phases within extended volumes may be associated with process control (pharmaceutical, cement etc.) and other industrial demands, which also extends to the identification of narcotics and a wide range of homemade explosives (HMEs) within complex "everyday objects". This problem requires a cost-effective material specific probe to enhance rapid false-alarm resolution,[3,14].

Focal construct technology (FCT),[15-18] is a technique, which employs an annular or conical shell beam of radiation designed to improve upon the aforementioned limitations. When such a

[a] *Imaging Science Group, Nottingham Trent University, Nottingham, UK.*
[b] *Cranfield Forensic Institute, Cranfield University, UK.*
Email: paul.evans@ntu.ac.uk
† Footnotes relating to the title and/or authors should appear here.
Electronic Supplementary Information (ESI) available: [details of any supplementary information available should be included here]. See DOI: 10.1039/x0xx00000x

beam is incident normally upon a semi or polycrystalline material, Debye cones with a well understood energy and angle relationships are produced from every point within the gauge volume formed by the intersecting beam in the sample. These cones overlap downstream in the imaging chain resulting in significantly increased diffracted flux intensity along the symmetry axis of the interrogating X-ray beam. This intensity increase is unique to FCT and cannot be replicated using a pencil or linear slit collimated beam[15-18]. In addition, FCT has been shown to deal favourably with non-ideal samples such as those exhibiting large grain size, preferred orientation,[16] and short-range structure order,[19] including liquids. Early incarnations of FCT employed a mono-energetic, angular-dispersive model, which resulted in Debye cones forming high intensity diffraction caustics,[15] measured with an area detector. This angular-dispersive approach has also been adapted into a tomographic technique employing raster scanning,[20]. More recently we have been able to extend this method to work in an energy-dispersive mode (i.e. ED-FCT),[21] by employing a polychromatic X-ray beam and energy-resolving point detector, resulting in further reductions in measurement time (i.e. 0.15 mAs).

Building on these techniques we introduce a new conceptual architecture (See Fig. 1) based on ED-FCT to identify materials distributed at unknown locations within an inspection volume.

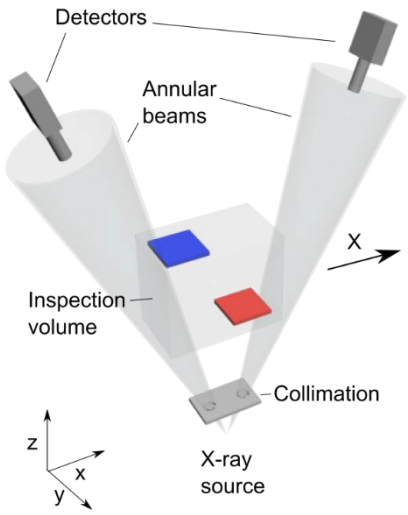

Fig 1. Conceptual dual beam focal construct imaging architecture employing a pair of conical shell primary X-ray beams each optically coupled to an energy-resolving point detector. The detectors are positioned at the centre of the dark area encompassed by each respective beam. The samples under inspection are translated linearly along the X-axis.

In this method the samples are translated through a pair of conical shell beams (with divergent symmetry or principal axes) derived from a single point X-ray source. The diffracted flux is measured by two energy resolving point detectors with a detector positioned on the symmetry axis of each beam. A powerful aspect of this technique is that diffracted flux measurements may be treated as if the beams had intersected physically or converged within the inspection volume,[22]. In effect, two temporally offset "perspective views" would be collected over the inspection volume thus enabling the material characteristics (e.g. d-spacings) and Z-axis position (or depth) dependency to be uncoupled. In principle, a point X-ray source can be used implement this architecture via appropriate geometric registration of signatures through post processing.

To emulate the functionality of the divergent dual beam architecture shown in Figure 1, our experiments employ a single stationary beam where the sample is scanned at two different tilt or angular positions relative to the beam. This scenario is also represented equivalently by two "cross firing" beams (see Fig. 3a). Each single beam scan enables match coefficients to be mapped onto the (Z,X) plane (See Fig. 2a and b). The material phase of a sample may be identified via calculation of d-spacings following Bragg's Law $\lambda = 2d \sin\theta$ where the wavelength λ, is obtained from the measured energy E, using Plank's energy-frequency relationship. The calculation of $\theta = f(Z, L, \Phi)$ is a function of the known geometric system parameters, where Z is the source-to-sample distance, L is the source-to-detector distance and Φ is the half-opening angle of the interrogating annular beam. It should be noted that interplanar spacings cannot be calculated uniquely using a single beam,[23] without *a priori* knowledge of the sample's axial position Z (i.e. an unknown Z equates to a range of possible d-spacing values per energy measurement, see Equation (1)).

As a proof-of-concept experiment, a volumetric sample was constructed containing a 30x30x5 mm^3 (x,y,z) thick vial of calcite and a 30x30x2 mm^3 (x,y,z) sheet of copper. The samples were configured parallel to the X-axis (i.e. motion direction) as well as being offset along the X-axis and Z-axis, respectively. An annular beam with a half-opening angular range of 3.92° ± 0.05° was produced by collimating the solid angle emission from a Hamamatsu micro-focus X-ray source operating at 130 kV, 300 μA with a bespoke tungsten optic.

Scattered rays were detected using an Amptek CdTe X-ray spectrometer with a 9 mm^2 circular detector with a typical full width at half maximum (FWHM) of 850 eV at 120 keV. The detector was placed at L = 510 mm from the X-ray source spot. The samples under inspection was translated 150 mm along the X-axis in 5 mm steps through the annular beam. To investigate the effect of the angular separation between the principal axes of the two beams the inspection volume was scanned at different rotations α, of ± 5°-20° in 5° increments. To investigate the effect of exposure time each linear scan was repeated for time periods of; 1 s, 0.5 s and 0.1 s per translation position (equating to 0.3, 0.15 and 0.03 mAs per point).

The presence of a specified material in measurements from a single sample translation scan may be determined using a systematic trial and error approach. A range of d-spacing values are generated incrementally from detector energy bins at possible Z-planes, Z_s, with their associated diffraction angle, 2θ, satisfying the Bragg condition following,[21]:

$$d = \frac{\lambda}{2\sin\left(\frac{1}{2}\left(\tan^{-1}\left(\frac{Z_s \tan\phi}{L - Z_s}\right) + \phi\right)\right)} \quad (1)$$

The consequent trial diffractogram is compared quantitatively to a specified material standard diffractogram through Pearson's correlation coefficient. A map is generated of the corresponding correlation coefficient for each assumed Z-plane location and translation position along the X-axis. Figure 2 illustrates the result of such an approach by comparing diffractograms with copper (See Fig. 2a) and calcite (See Fig. 2b) standards. Some example diffractograms that illustrate good correspondence with the standards are illustrated in Figure 2c and d for copper and calcite, respectively. The 'true' locations of the copper and calcite samples in these maps are indicated by the red and blue boxes, respectively. It can be seen that this method favourably identifies the locations of the sample materials. A correlation coefficient >0.75 highlights correct matches but also includes several ambiguous positions (particularly for copper, See Fig. 2a) that also yield high match coefficients, which could lead to false positives. These are likely the result of copper's cubic crystal structure, which results in a high degree of symmetry in its diffractogram.

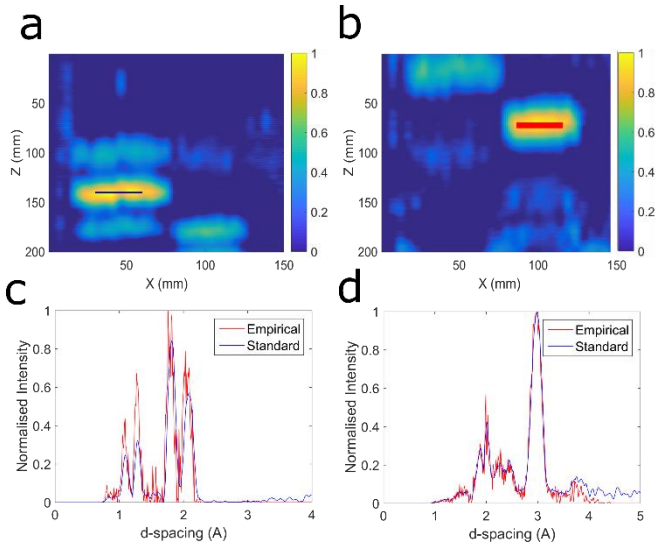

Fig 2. Match coefficients mapped onto the (Z,X) plane are created by comparing empirical diffractograms against a copper (a) and calcite (b) standard. The true locations of the copper and calcite samples are illustrated by the blue and red boxes, respectively. Example diffractograms illustrating good match coefficients are also illustrated for copper (c) and calcite (d).

To resolve erroneous sample positions the inspection volume must be described further. Our (single beam) dual-scan set-up emulates the conceptual (dual beam) single-scan approach, whereby the inspection volume is scanned by two angularly offset beams ±α about a known point so that these scans interrogate the same 3D space but at different times. Considering two crossed, annular beams, rotated by $\pm\alpha$ and translated by $\pm\Delta X_{\mp\alpha}$ from the symmetry axis of the system, the cross-over location C, can be derived analytically from the geometry following:

$$(x_0, z_0) = \left(0, \frac{2\Delta x_\alpha}{\tan(\alpha + \phi) + \tan(\alpha - \phi)}\right) \quad (2)$$

Applying the trial and error approach (described previously) results in two match coefficient (Z,X) plane maps with a known transformation between their respective coordinate systems as described in Equation (3). The required transformation is a rotation about point C by $\pm\alpha$ for respective sample rotations, $\mp\alpha$.

$$\begin{pmatrix} x_{\pm\alpha} - x_0 \\ Z_{\pm\alpha} - Z_0 \end{pmatrix} \begin{pmatrix} \cos(\mp\alpha) & -\sin(\mp\alpha) \\ \sin(\mp\alpha) & \cos(\mp\alpha) \end{pmatrix} + \begin{pmatrix} x_0 \\ Z_0 \end{pmatrix} = \begin{pmatrix} x_{\pm\alpha}' \\ Z_{\pm\alpha}' \end{pmatrix} \quad (3)$$

Where (x_0, z_0) represents the cross-over location C of the two beams aligned according to a common coordinate system. The maps can then be overlaid to calculate the product of the left- and right-rotated scans' match coefficients. True positive results are subsequently reinforced and false positives become weakened (see Fig. 3b and c).

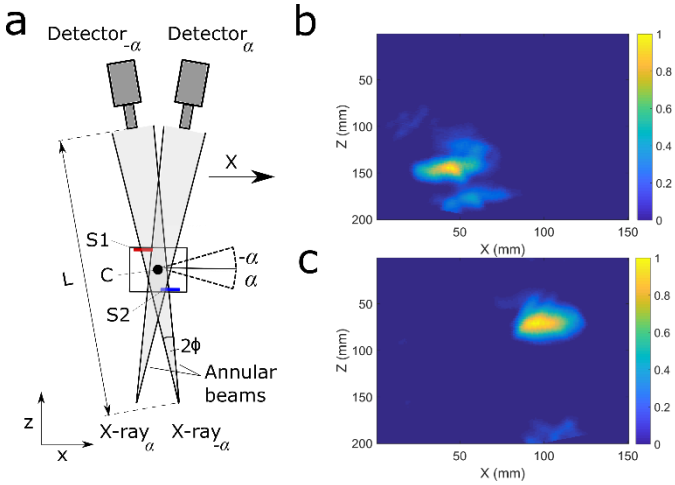

Fig 3. Schematic of two "cross-firing" conical shell beams (a) and the reinforced match coefficient maps for copper (b) and calcite (c) for α= ±20° sample tilt angles (equivalent to a relative beam rotation) aligned to a common coordinate system.

To optimise our arrangement, we have investigated a range of exposure times and rotation angles α. Match coefficient maps for copper and calcite samples are illustrated in Figure 4. Reduction in exposure times are represented in Figures 4a-c, respectively.

Decreasing the exposure time per scan is accompanied by a non-linear decrease in the value of match coefficients. For example, decreasing from 1 s per point to 0.1 s per point results in a match value decrease of ~5%. Uncertainties in d-spacing for a related system architecture have been described in detail elsewhere,[21]. However, the method reported in this paper also estimates axial sample position.

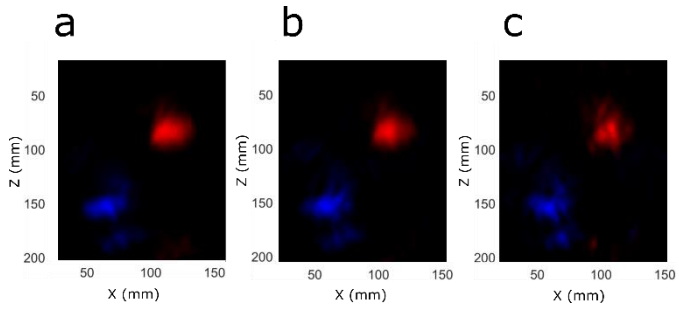

Fig 4. Match coefficient maps for copper (blue) and calcite (red) exposed for 1 (a), 0.5 (b), 0.1 (c) seconds exposure per translation point. The raw data was obtained using a dual-scan and sample rotations $\alpha = \pm 20^{o}$.

Experimentally we find the uncertainty in depth tends to reduce with increasing rotation α. This characteristic was expected as it is consistent with applying triangulation techniques to calculate axial position or range,[22]. The uncertainty in depth $\Delta Z \sim 10$ mm was estimated from the experiment match coefficient maps for the (Z,X) plane with reference to the true axial positions.

Conclusions

In summary, we demonstrate that our dual beam measurement architecture enables the characterisation of materials at unknown locations within extended volumes. This operational requirement is encountered routinely in many applications where material characteristics, such as phase and lattice parameters are critical.

In our proof-of-principle experiment we employ a tilted-sample dual-scan with a single stationary annular beam to emulate the measurements possible using a dual-beam single scan. An energy resolving point detector positioned at the centre of the dark area encompassed by the beam provides diffracted flux measurements from interrogated samples. Specifically, by comparing the range of possible material signatures, predicted by the known geometric configuration and the measured energies, from each "different beam" enables the axial location and d-spacing relationship to be decoupled. True positive material identification/locations are subsequently reinforced while false positives become weakened.

By hypothesis the angular offset between the two beams along the scan direction may be realised using a single point source fitted with appropriate optics. Critically, this configuration negates the requirement for two separate "cross firing" X-ray generators producing physically intersecting beams. In addition, a dual-beam single source solution would reduce the cross coupling of scattered X-rays from the "other beam" by virtue of the increased linear separation between the point detectors (i.e. from inverse-square law and Bragg law considerations).

While our work supports the promise of a cost-effective and compact high-energy X-ray diffraction scanner technology there remains much work to be done. For example, in principle, it is feasible to produce a series of annular beams using a single point X-ray source promising significantly improved matching and scan speeds. We anticipate such a multibeam technique would be advantageous for samples with relatively large Z-axis thickness or flat samples, which are not parallel to the motion or X-axis i.e. presenting significantly different "beam path thickness" to each interrogating beam.

Our proposed technique is scalable with respect to both scan size and X-ray energy and is, in principle, capable of rapid depth-resolved materials characterisation of bulk samples or objects. These ideas and preliminary results are especially expedient given the growing need for rapid volumetric materials identification in fields such as explosives detection, diagnostic and biological imaging, and process control.

Acknowledgements

This work was funded by the Department of Homeland Security, Science and Technology Directorate, Homeland Security Advanced Research Projects Agency, Explosives Division through the Advanced X-ray Material Discrimination Program; contract HSHQDC-15-C-B0036

Conflicts of interest

There are no conflicts to declare.

Notes and references

1 W.C. Rontgen, *Nature,* 1896, **53,** 274-277.
2 S. Huotari, T. Pylkkanen, R. Verbeni, G. Monaco and K. Hamalainen, *Nature Materials*, 2011, **10,** 489-493.
3 G. Harding, *Applied Radiation and Isotopes*, 2012, **70** (7) 1228-1237.
4 K. MacCabe, K. Krishnamurthy, A. Chawla, D. Marks, E. Samei and D. Brady, *Optics Express,* 2012, **20**(15), 16310-16320.
5 Z. Zhu, A. Katsevich, A. J. Kapadia, J. A. Greenberg and S. Pang, *Scientific Reports, 2018,* **8**, 522.
6 J. A. Greenberg, M. Hassan, K. Krishnamurthy and D. Brady, *Analyst*, 2014, **179** 709-713
7 D. O'Flynn, C. Crews, I. Drakos, C. Christodoulou, M. D. Wilson, M. C. Veale, P. Seller and R. D. Speller*, J. Phys. D: Appl. Phys, 2016,* **49**(17), 175304-175213.
8 M. Hassan, J. A. Greenberg, I. Odinaka and D. J. Brady, *Opt. Express*, 2016, **24**(16), 18277-18289.
9 S. Zhou and A. Brahme, *Physica Medica*, 2008, **24** 129-148.
10 A. Greenberg, K. Krishnamurthy and D. Brady*, Opt. Express*, 2013, **21**(21), 25480-25491.
11 S. F. Neilsen, E. M. Laurisden, D. Juul Jensen and H. F. Poulsen, *Materials Science and Engineering A,* 2001, **319-321**. 179-181.
12 R. J. Cernik, K. H. Khor and C. Hansson, *Journal of the Royal Society Interface*, 2008, **5**. 477-481.
13 O. Lazzari, S. Jacques, T. Sochi and P. Barnes, *Analyst*, 2009, **134**, 1802-1807.
14 K. Wells and D. A. Bradley, *Appl. Radiat. Isot,* 2012, **70**(8), 1729-1746.
15 P. Evans, K. Rogers, J. Chan, J. Rogers and A. Dicken, *Applied Physics Letters*, 2010, **97**, 240101.
16 K. Rogers, P. Evans, J. Rogers, J. Chan and A. Dicken, *Journal of Applied Crystallography*, 2010, **43**, 264-268.

17 F. Li, Z. Liu, T. Sun, B. Jiang and Y. Zhu, *J. Chem. Phys*, 2016, **144** 104201.
18 F. Li, Z. Liu and T. Sun, *Journal of Applied Crystallography*, 2016, **49**, 1-5.
19 D. Prokopiou, K. Rogers, P. Evans, S. Godber and A. Dicken, *Applied Radiation and Isotopes*, 2012, **77**, 160-165.
20 P. Evans, K. Rogers, A. Dicken. S. Godber and D. Prokopiou, *Optics Express*, 2014, **22**, 11930-11944.
21 A. J. Dicken, J. P. O. Evans, K. D. Rogers, C. Greenwood, S. X. Godber, D. Prokopiou, N. Stone, J. G. Clement, I. Lyburn, R. M. Martin and P. Zioupos, *Optics Express*, 2015, **23**(10), 13443-13454.
22 J. P. O. Evans, *Institute of Physics Journal of Measurement Science and Technology*, 2002, **13**, 1388-1397.
23 A. J. Dicken, J. P. O. Evans, K. D. Rogers, N. Stone, C. Greenwood, S. X. Godber, D. Prokopiou, J. G. Clement, I. D. Lyburn, R. M. Martin and P. Zioupos, *Phys. Med. Biol.* 2015, **60**, 5803–5812.